AIAA Propulsion and Energy Forum
July 9-11, 2018, Cincinnati, Ohio
2018 Joint Propulsion Conference

10.2514/6.2018-4730

Observation of Low Frequency Plasma Oscillations in the Plume of a Partially Magnetized Magnetic Nozzle

Shadrach T. Hepner*
University of Michigan, Ann Arbor, MI, 48109

Benjamin N. Wachs†
University of Michigan, Ann Arbor, MI, 48109

Timothy T. Collard‡
University of Michigan, Ann Arbor, MI, 48109

Benjamin A. Jorns§
University of Michigan, Ann Arbor, MI, 48109

The density fluctuations in the plume of a 50 W, partially-magnetized magnetic nozzle source are experimentally and analytically characterized. A pair of ion saturation probes arrayed in the horizontal direction are employed to generate both power spectra and dispersion relations for fluctuations ranging from 0-1 MHz in the magnetic nozzle plume. Spatially resolved measurements are performed for a 30W, 1 sccm-Xe operating condition. Plasma instabilities with linear dispersions are observed with Beall analysis, and employing a quasilinear theory, their amplitudes are correlated with an effective anomalous collision frequency that can facilitate cross-field transport. It is found that the anomalous collision frequency from these waves is an order of magnitude more significant than the classical electron-neutral collisionality in the downstream region. This finding is discussed in the context of mechanisms for electron detachment.

I. Nomenclature

P_e	=	Electron pressure
q	=	Electron charge
n	=	Plasma density
$\vec{E}$	=	Electric field
$\vec{u_e}$	=	Electron fluid velocity
$\vec{B}$	=	Magnetic field
ν_e	=	Classical electron collision frequency
m_e	=	Electron mass
u_i	=	Ion fluid velocity
Ω_e	=	Hall parameter
F_{AN}	=	Anomalous force
i_{sat}	=	Ion saturation current
T_e	=	Electron temperature
ω	=	Wave angular frequency
k	=	Wavenumber

*AIAA Junior Member, Ph.D. Candidate, Plasmadynamics and Electric Propulsion Laboratory, Department of Aerospace Engineering, shadrach@umich.edu.
†AIAA Junior Member, Ph.D. Candidate, Plasmadynamics and Electric Propulsion Laboratory, University of Michigan, Department of Aerospace Engineering, bwachs@umich.edu.
‡AIAA Junior Member, Ph.D. Candidate, Plasmadynamics and Electric Propulsion Laboratory, Department of Aerospace Engineering, collardt@umich.edu.
§AIAA Senior Member, Assistant Professor, Plasmadynamics and Electric Propulsion Laboratory, Department of Aerospace Engineering

ω_{pe}	=	Plasma frequency
ω_{pi}	=	Ion plasma frequency
ϕ	=	Plasma potential
A_{probe}	=	Probe surface area
c_s	=	Ion sound speed
n_n	=	Neutral number density
σ	=	Electron-neutral cross section

II. Introduction

Partially magnetized magnetic nozzles (MNs) are type of electric propulsion technology currently being researched that operate by accelerating a plasma through a diverging magnetic field, thereby converting thermal energy to directed thrust [1–4]. The plasma source is typically electrodeless, generating plasma from a radiofrequency or microwave antenna. The applied magnetic field limits interactions between the plasma and the walls, allowing MNs to theoretically have extremely long lifetimes. Furthermore, because of the lack of contact between an electrode and the plasma, they are able to perform on more corrosive propellants. This characteristic makes them a candidate for missions requiring in-situ refueling or for dual mode operation where the propellant could be ignited chemically for high thrust or propelled electrically for high specific impulse. While they provide a potential means for extended missions, the physics behind their operation is not yet fully understood.

A primary question regarding the operation of MNs is that of plasma detachment. The nature of direct current magnetic fields or permanent magnets imply that all but the centermost magnetic field line will form a closed loop because of the nonexistence of magnetic monopoles. As such, the plasma may remain attached to the fields and return to the thruster without a mechanism for detachment. Since electrons and ions behave differently in the expanding magnetic field, this detachment process may occur in each of these species separately. In partially magnetized plasmas, ions are minimally influenced by the magnetic fields since they are more inertial and thus have a larger Larmor radius. Ion motion is rather determined by the electric fields imposed by charge separation. Ion detachment has been studied extensively and is considered well understood [5]. However, the models for ion detachment assume fully magnetized electrons. This assumption cannot be physical, since it implies a negative charge buildup once the electrons return, which would negate the electric field accelerating the ions. As electrons follow the field lines past the point of ion detachment, electric fields form between the two species. If electrons are too strongly attached to the magnetic fields, the ions will follow the electrons back towards the thruster, generating no net thrust. Thus, for MNs to produce thrust, some mechanism must exist for electrons to detach from magnetic field lines.

Electron detachment from MNs has been studied previously from both theoretical and experimental standpoints. Hooper proposed that finite electron inertia would yield a detachment scenario, proposing that finite electron inertia would imply convergent electron detachment, collimating the beam. However, it has since been shown that finite electron inertia in fact yields divergent detachment, further separating the electrons and ions [6]. Arefiev [7] has proposed detachment based on magnetic field line stretching. This mechanism relies on the presence of paramagnetic electron drifts, which are currently believed not to exist in standard low ion temperature magnetic nozzles based on experimental evidence [8]. Furthermore, resistive detachment caused by collisions between electrons and ions [9] or electrons and neutrals [10] provides a further mechanism for outward separation. This mechanism depends on a low ionization fraction, and we do not expect this mechanism to be significant as we continue to optimize design of MNs. Finally, plasma instabilities have been proposed to provide an additional mechanism for electron detachment [9, 11]. Similarly to resistive detachment, the anomalous resistivity induced by instabilities will depend on the direction of the electron drift. If currents are indeed universally diamagnetic, the instabilities will work to further diverge the ion beam and worsen performance of the thruster. The need is apparent to further understand the influence of the instabilities on electron detachment to better predict how the plasma motion will evolve throughout the plume.

In this experiment, we map the presence of low-frequency instabilities with linear dispersion in the plume of a low-power partially magnetized MN and discuss their impact on detachment. This paper is organized in the following manner: Section III presents theoretical background behind the physics we present, Section IV presents the experimental setup we used in this experiment, SectionV presents our probe findings, and Section VI discusses the primary implications of our findings on electron cross-field mobility and detachment.

III. Background

Classical electron-neutral collisions have been shown to correlate to upstream detachment previously [10]. As electrons orbit in the azimuthal direction, their collisions with neutrals provide a drag force. We can use the electron Ohm's Law to describe this motion:

$$0 = -\nabla P_e - qn(\vec{E} + \vec{u}_e \times \vec{B}) - \nu_e m_e n(\vec{u}_e - \vec{u}_i) \tag{1}$$

where P_e is the electron pressure, q is the electron charge, n is the plasma density, $\vec{E}$ is the electric field, u_e is the electron fluid velocity, ν_e is the electron collision frequency, m_e is the electron mass, $\vec{u}_i$ is the ion fluid velocity. Taking the cross product of the magnetic field with Equation 1,

$$0 = -\nabla P_e \times \vec{B} - qn\vec{E} \times \vec{B} - qn\left[(\vec{u}_e \cdot \vec{B})\vec{B} - B^2\vec{u}_e\right] - \nu_e m_e n(\vec{u}_e - \vec{u}_i) \times \vec{B}. \tag{2}$$

We now define an orthogonal coordinate system $\hat{x}, \hat{y}, \hat{z}$ such that $\vec{B} = B\hat{z}$ with symmetry in the $\hat{x}$ direction, i.e. $\frac{\partial}{\partial x} = 0$. Taking the $\hat{y}$ component of Equation 2 and assuming that ion motion perpendicular to the magnetic field is small yields

$$u_{e,y} = \frac{\nu_e m_e u_x}{qB} \tag{3}$$

implying that the drag force from electron collisionality can induce electron motion perpendicular to the magnetic field. We can further replace u_x by taking the $\hat{x}$ component of Equation 2:

$$u_{e,x} = \frac{\nu m_e u_{e,y}}{qB} + \frac{\partial P_e/\partial y}{qnB} - \frac{E_y}{B}. \tag{4}$$

Combining 3 and 4 then yields

$$u_{e,y} = \frac{\frac{\partial P/\partial y}{qnB} - \frac{E_y}{B}}{\Omega_e + 1/\Omega_e} \tag{5}$$

where we have defined the Hall parameter $\Omega_e = \frac{qB}{m\nu_e}$ as the ratio of the electron gyrofrequency to the collision frequency. Equation 5 shows that a finite resistivity can cause cross-field transport. Further, it predicts the direction of the transport as the difference between the diamagnetic drift velocity $v_D = \frac{\partial P/\partial y}{qnB}$ and the $E \times B$ velocity, $v_E = \frac{E_y}{B}$.

We now hypothesize an extra force included into Equation 1, which we call F_{AN}. The electron Ohm's law now becomes

$$0 = -\nabla P_e - qn(\vec{E} + \vec{u}_e \times \vec{B}) - \nu_e m_e n(\vec{u}_e - \vec{u}_i) - nF_{AN}. \tag{6}$$

Following the same process, we determine a new equation for $u_{e,y}$:

$$u_{e,y} = \frac{\frac{-\partial P/\partial x}{qnB} - \frac{E_x}{B} - \frac{1}{\Omega_e}\frac{F_{AN,y}}{qB} - \frac{F_{AN,x}}{qB}}{1 + \frac{1}{\Omega_e^2}} \tag{7}$$

where we have recovered Equation 5 with two extra terms involving the anomalous force. This relation implies that an anomalous force can enhance cross-field electron transport in similar ways to classical collisionality.

The presence of instabilities can yield such an anomalous force term in addition to the classical term. Instabilities have previously been shown to cause cross-field transport in various electric propulsion devices, which can be modelled by an anomalous collision frequency ν_{AN}, [12–15] and have been theorized to cause similar transport in magnetic nozzles [9, 11]. Observing these waves and assuming properties about the plasma, we can define the anomalous collision frequency. We may then compare this value to classical electron-neutral collisions to determine where each term is significant throughout the MN plasma.

IV. Experimental Setup

In this section, we present our means of measuring wave presence and background plasma parameters in an MN. In particular, we need a vacuum chamber and thruster on which to perform measurements, diagnostics to characterize the frequency and wavenumber of the waves, and electrostatic probes to measure the number density and plasma potential throughout the plume to describe our observations theoretically. Figure 1 presents the setup we used throughout this experiment.

A. PEPL ECR Thruster

We performed our experiment on the PEPL Electron Cyclotron Resonance (ECR) Thruster developed at the University of Michigan based off of the MINOTOR design by Onera [16]. The PEPL ECR Thruster consists of a 27.5 mm diameter exit plane with a centrally mounted monopole antenna. We drive the antenna at 2.4 GHz to generate and heat a plasma within the aluminum casing and accelerate it axially with a diverging magnetic field imposed by permanent magnets. The thruster is capable of operating at powers down to 1 W and flow rates as low as 0.1 SCCM Xenon. In the current work, we operated at 30W/1sccm-Xe.

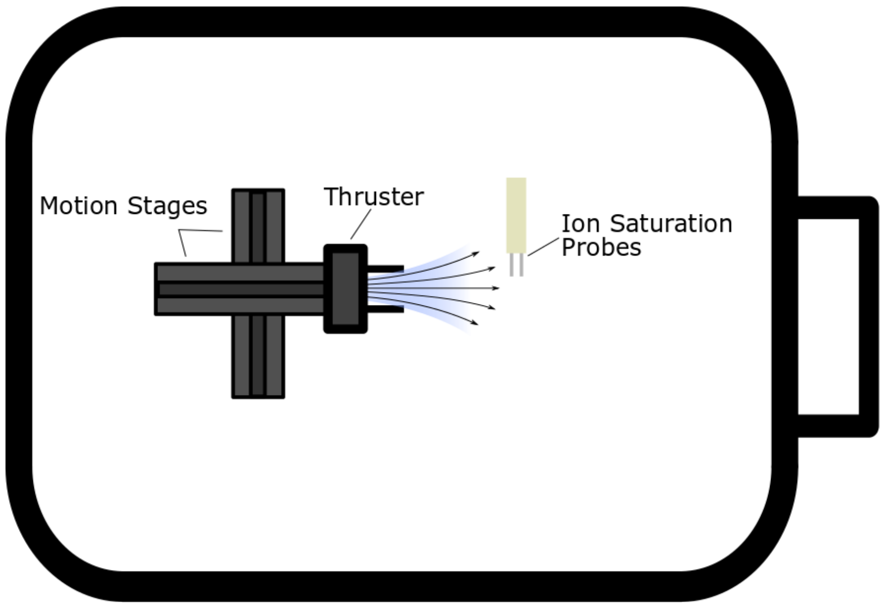

Fig. 1 PEPL ECR Thruster in the Junior Test Facility on bidirectional motion stages and ion saturation probes.

B. Junior Test Facility

We performed our experiment in the Junior Test Facility at the Plasmadynamics and Electric Propulsion Laboratory at the University of Michigan. Junior is 3m in length and 1m in diameter. It is capable of 30,000 L/s pumping speed on Xenon by use of a turbopump and cryopump. In this experiment, we operated at a backpressure of 5.3×10^{-6} Torr.

C. Planar Langmuir Probe

To determine the plasma potential, we swept a tungsten planar Langmir probe 2mm in diameter throughout the plume. We swept the probe from -200V to 200V and determined the plasma potential by finding the knee of the current-voltage characteristic. We further determined the beam current density by taking the reading at -160 V as the ion saturation current. While there was likely significant sheath expansion farther downstream, the ion saturation area of the sweep became nonlinear at biases closer to zero.

D. Ion Saturation Probes

Ion saturation probes provide a means of measuring the presence of plasma waves based on the following analysis [17]. First, we note that the ion saturation current can be decomposed into a time averaged component and a varying component,

$$i_{sat}(t) = \bar{i}_{sat} + \tilde{i}_{sat} \tag{8}$$

$$\frac{\tilde{i}_{sat}(t)}{\bar{i}_{sat}} = \frac{i_{sat}(t)}{\bar{i}_{sat}} - 1. \tag{9}$$

Now, noting that $\bar{i}_{sat} = 0.61 A_{probe} n_0 q \sqrt{T_e/m_i}$ for a cylindrical probe and assuming that electron temperature does not change significantly over time, we see that

$$\frac{\tilde{i}_{sat}(t)}{\bar{i}_{sat}} = \frac{\tilde{n}}{n_0} \tag{10}$$

where $\tilde{i}_{sat}$ is the time-varying ion saturation current, $\bar{i}$ is the time averaged ion saturation current, $\tilde{n}$ is the time varying ion density and n_0 is the time averaged ion density. For electrostatic oscillations, we can relate the fluctuations in number density to plasma potential with the following, derived from the Boltzmann equation after assuming that potential oscillations are much lower in magnitude than the electron temperature:

$$\phi \approx \frac{T_e}{q}\frac{\tilde{i}}{\bar{i}}. \tag{11}$$

Here ϕ is the plasma potential oscillation. Thus far, we have been measuring solely in terms of time and space. However, we can define coherent waves in terms of a frequency and a wavenumber. Applying an inverse Fourier transform, we see,

$$\phi(t,x) = \int_\omega \frac{d\omega}{2\pi}\Phi(\omega, x)\exp(-i\omega t) \tag{12}$$

$$= \int_\omega \frac{d\omega}{2\pi}\int_k \frac{dk}{2\pi}\Phi(\omega, k)\exp(ikx - i\omega t) \tag{13}$$

Here, the coefficient $\Phi(\omega, k)$ describes the frequency-wavenumber components of the wave, k is the wavenumber, and ω is the angular frequency. A single probe can be used to determine the coefficients in Equation 12, but we must use a second probe to determine the coefficients in Equation 13. We assume that the waves maintain a constant ω and k while propagating between the two probes, and thus the only difference in measurement between the two probes is in the exponential term, i.e. the phase offset. If we trigger both measurements simultaneously, the difference in phase that we will observe, $\Delta\theta$, is only the result of the spatial distance between the probes and the wave number, i.e. $\Delta\theta = k(x_2 - x_1)$. As we know the probe locations beforehand, we can use the $\Delta\theta$ that we observe to calculate k.

Furthermore, assuming these probes are fully in ion saturation, we can estimate the number density of the plasma. We take the mean current read by the probes and apply cylindrical Langmuir probe theory,

$$I_{sat} = 0.61 A_{probe} n_i q \sqrt{T_e/m_i}. \tag{14}$$

Here, A_{probe} is the probe area and I_{sat} is the ion saturation current. After finding the number density from each probe, we take the mean of the two and declare the result as the ion number density at that point.

In this experiment, we used two probes 0.7 mm in diameter and 5mm in length oriented 5mm apart in the azimuthal direction. We biased each to -36 V using four nine volt batteries to ensure that the probes were collecting ion saturation current, allowing us to apply Equation 11. We measured at a rate of 2 megasamples/second for 0.5 seconds. We then binned the data into 100 equal-sized bins to reduce noise.

V. Results

A. Planar Langmuir Probe

Figure 2 presents the current density measurements through the plume. There is an off-axis peak between zero and 10 mm in the radial direction, followed by a steady decrease farther outwards. The progression and eventual disappearance of the off-axis peak is evidence of a sustained attachment for at least a centimeter until the ion streamlines are able to converge on centerline.

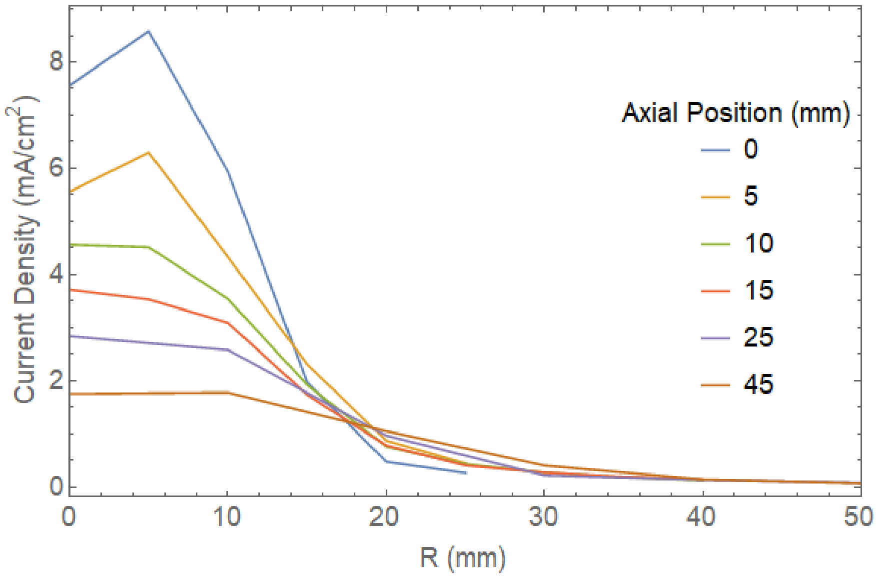

Fig. 2 Radial sweeps of current density at varying axial locations for all four operating conditions.

Figure 3 presents the plasma potential determined by the Langmuir probe. Mirroring the beam current data, the plasma potential indicates a slight potential well on centerline. We found the potential by plotting the I-V characteristic on a logarithmic scale and finding the knee of the curve.

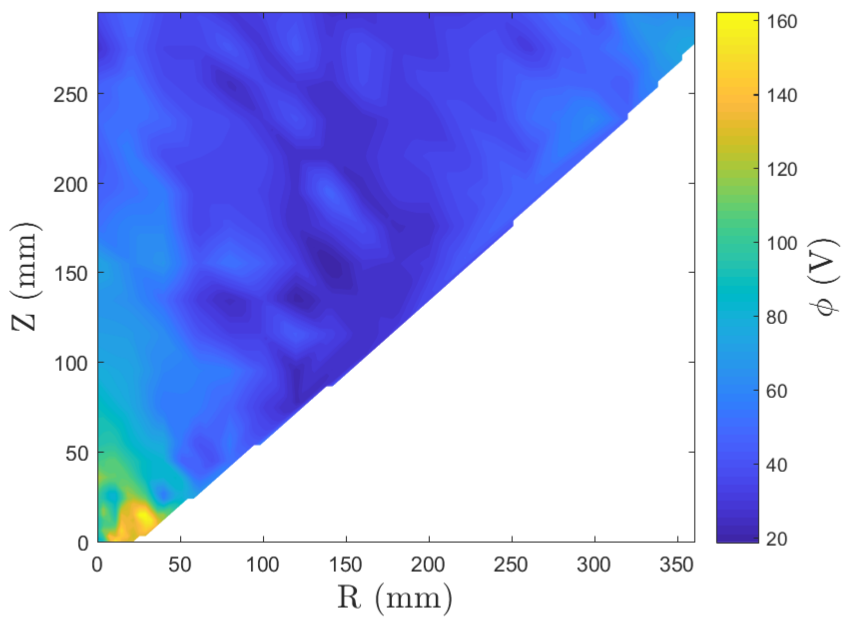

Fig. 3 Contours of plasma potential throughout the plume for each condition (V).

B. Number Density

Figure 4 presents the number density results from the ion saturation probe measurements. We find the number density peak to be 2.9×10^{17} m^{-3}. Again, we observe that this peak appears 5-10 mm away from centerline close to the thruster and extends outwards downstream.

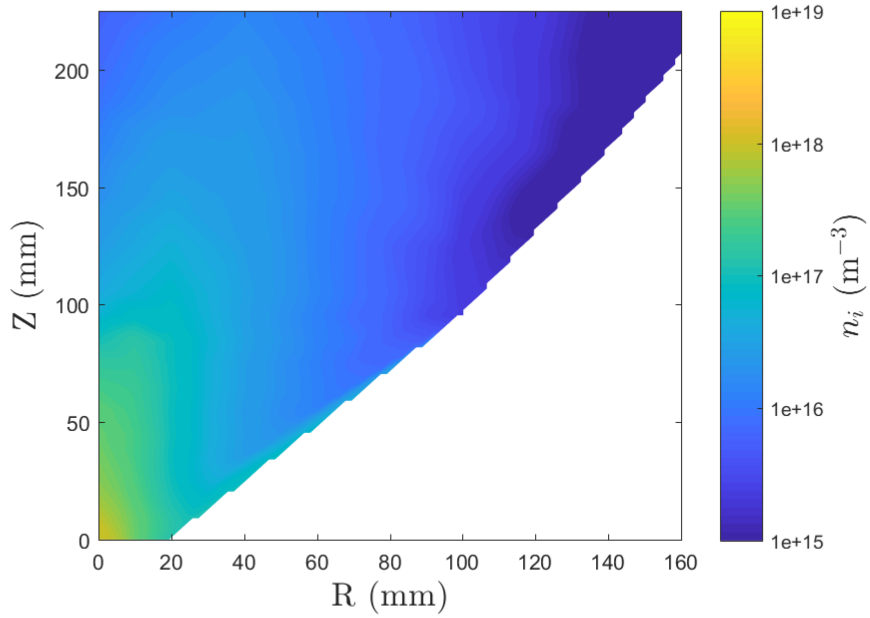

Fig. 4 Contour of ion number density throughout the plume.

C. Neutral Density Simulations

To estimate the significance of electron-neutral collisions, we estimate the neutral density using COMSOL. Since we predict the ion fraction to be low, we neglect ionization and assume that the background density is the same when the plasma is present. We do not present the results here; the reader is referred to the work by Wachs [18] for a full description of the neutral density.

D. Wave Measurements

We present in this section the results from the ion saturation probe measurements. We first discuss the interpretation of Beall Plots, then proceed to present the wave presence throughout the plume.

1. Beall Plots

Beall Plots represent the relative magnitude of the aforementioned coefficients $\Phi(\omega, k)$ graphically. The x-axis represents wave number, ranging from -600 to 600 m^{-1}, and the y-axis represents frequency, ranging here from 0 to 250 kHz. We measured saturation current at a sample rate of 2 Megasamples per second, yielding measurements up to 1 MHz. However, we did not see significant wave presence above 250 kHz, so we have limited our reporting to this value. Representing this data on such a plot provides a means of visualizing the dispersion relation $\omega(k)$. With the present representation, a positive k indicates propagation in the $\hat{z} \times \hat{r}$ direction. Figure 5 presents an example Beall plot with a negative slope. Such a phase velocity corresponds to paramagnetic propagation.

We present a map of all of the dispersion relations out to 120 mm in Figures 6 and 7.

We notice a faint linear dispersion in the positive θ direction, parallel to a diamagnetic electron drift, close to the thruster and aligning with the negative slope in number density presented in Figure 4.

Figure 8 presents the phase velocity ω/k throughout the plume. We represent only the waves with linear dispersion here and show the direction reversal by dashed black lines.

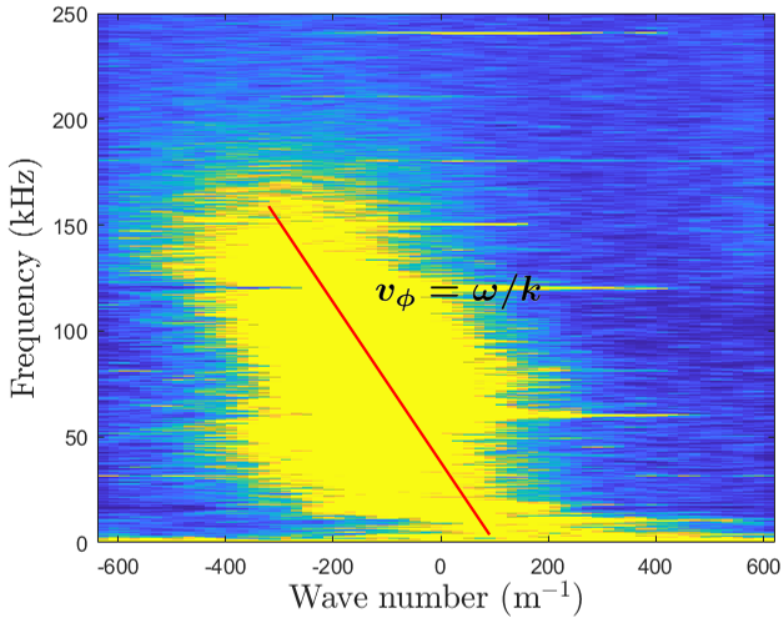

Fig. 5 Example Beall plot representing relative oscillation magnitude in frequency-wavenumber space. The red line indicates the phase velocity. The negative slope in this case corresponds to a paramagnetic drift motion.

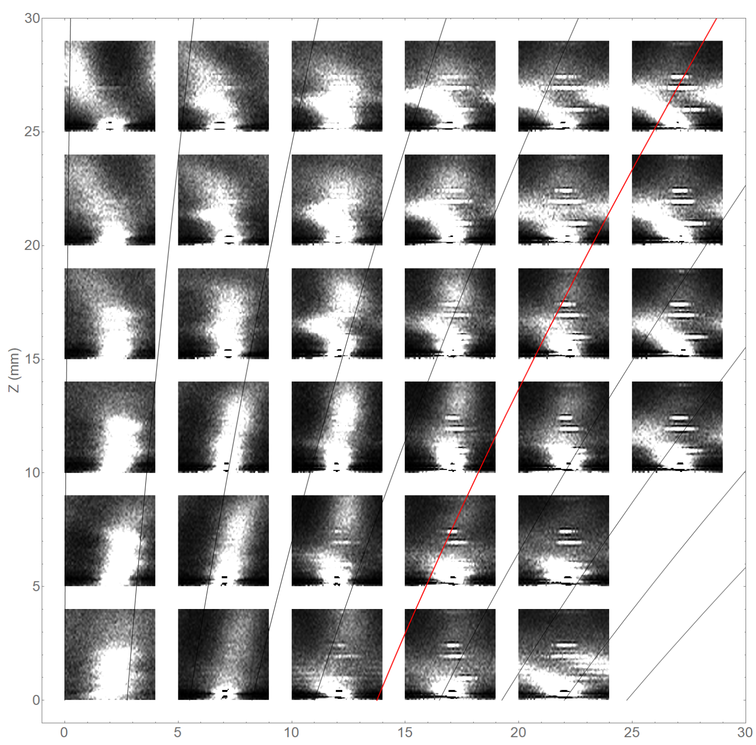

Fig. 6 Beall Plots throughout the plume up to 30 mm from the thruster. Plots are limited in frequency space to 250 kHz and range in wavenumber from -600 to 600 m^{-1}.

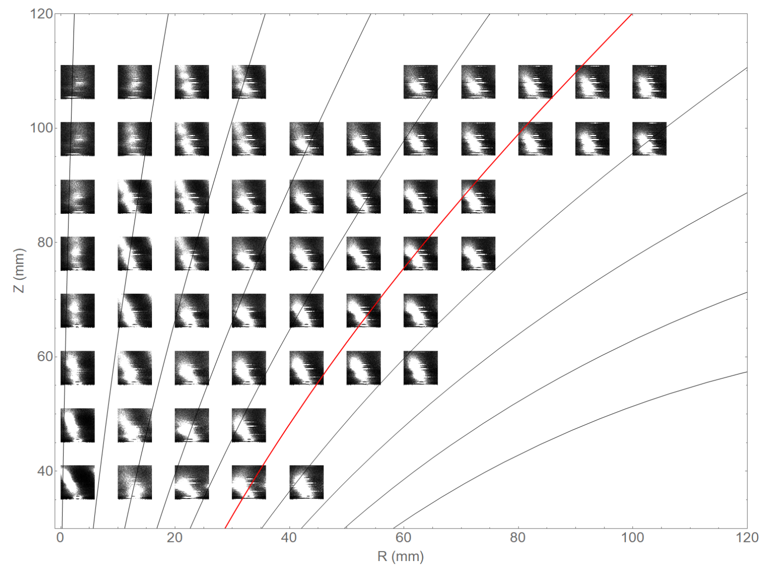

Fig. 7 Beall Plots throughout the plume past 30 mm from the thruster. Plots are limited in frequency space to 250 kHz and range in wavenumber from -600 to 600 m^{-1}.

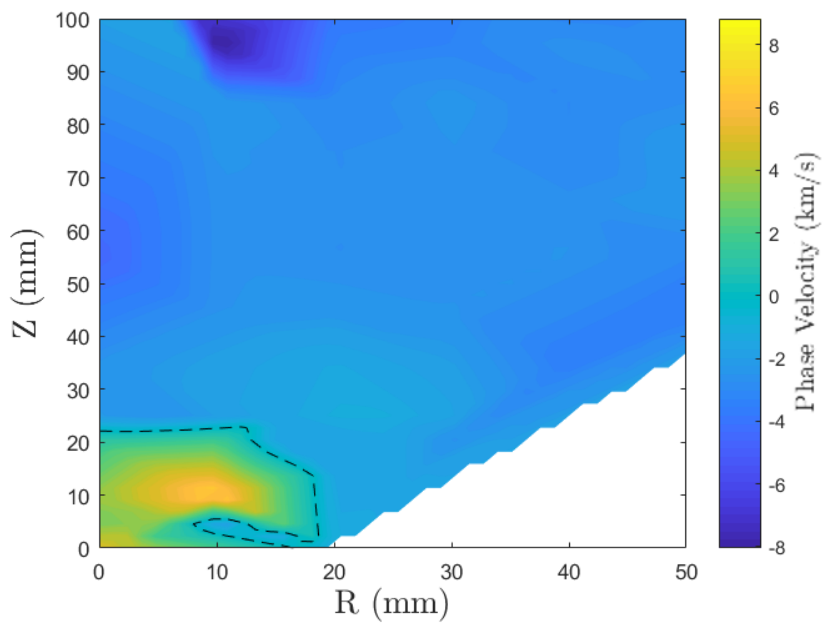

Fig. 8 Phase velocity of waves throughout the plume for all four operating conditions. Here, positive velocities represent propagation in the clockwise direction while looking downstream, and the dashed black line represents a transition from positive to negative values. We have removed points that did not exhibit linear dispersion.

It is clear that instabilities exist in the plume. We will now progress to discussing these waves theoretically and describing their impact on effective collision frequency.

VI. Discussion

In this section, we first discuss theoretical description of the waves we observe throughout the plume.

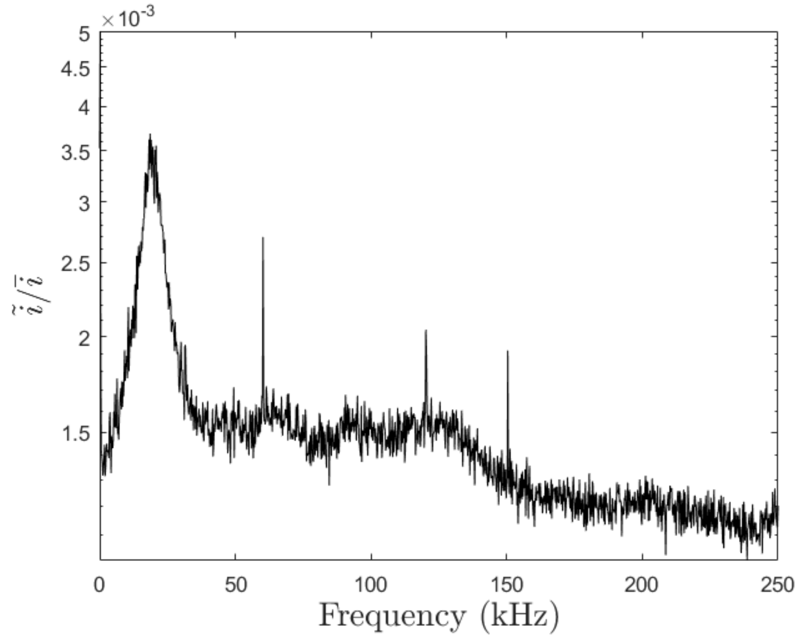

Fig. 9 Oscillation magnitude as a function of frequency at $R = 0$mm and $Z = 15$mm.

A. Theoretical Description

With the linear dispersion that we observe, we conjecture that these waves are acoustic-like instabilities. The dispersion relation of an acoustic-like wave takes the linear form $\omega/k \approx c_s$, where c_s is the ion sound speed, $c_s = \sqrt{T_e/m_i}$. While we do not yet have accurate electron temperature measurements in the plume, we can estimate a temperature based on MINOTOR [16] to be between 10 and 20 eV. Since we operate on Xenon, these values correspond to an acoustic speed of $\approx 3000 - 4000$ m/s. As we see from Figure 8, the phase velocities range between -4000 and 8000 m/s, with a few outliers. With this assumption, we can define the anomalous collision frequency as

$$\nu_{AN} = \frac{\omega_{pe}}{T_e^2} \sum_{\omega} (q\phi(\omega))^2 \tag{15}$$

[19] where T_e is the electron temperature, q is the electron charge, ω_{pe} is the plasma frequency, and $\phi(\omega)$ is the magnitude of plasma potential oscillations,

$$\phi = \frac{T_e}{q} \frac{\tilde{i}}{\bar{i}}. \tag{16}$$

Thus, knowing the oscillation magnitude of the ion saturation current along with plasma number density will provide us with what we need to estimate the anomalous collision frequency. Figure 9 presents a sample from the current experiment that presents the data we totaled. We take this sum over frequency space up to 250 kHz, where we were no longer able to observe the dispersion. We consider any contribution above 250 kHz to the anomalous collision frequency to be noise.

B. Impact on Detachment

Instabilities enhance cross field mobility and can lead to detachment. We consider them to enhance resistive detachment by yielding an anomalous collision frequency, given by Equation 15 for ion acoustic waves. The impact that this collisionality has on detachment depends on the direction of motion. In magnetic nozzles, it is the diamagnetic electron current that generates thrust, and these have been detected experimentally [8]. However, the resistive forces on these currents will also enforce diverging detachment, increasing ion divergence and decreasing device efficiency. A downstream paramagnetic drift would imply a resistive force that allows electrons to diffuse inwardly. Figure 10 depicts these two types of drifts. Assuming the phase velocity of the waves parallels the azimuthal velocity of the electrons, we

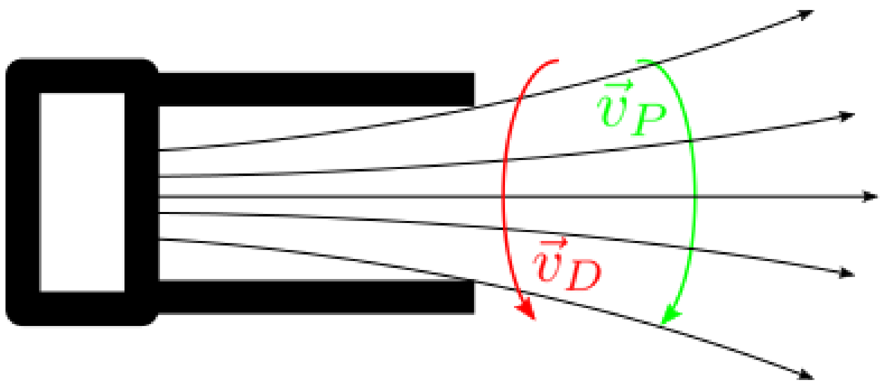

Fig. 10 Diamagnetic (v_D) and paramagnetic (v_P) electron currents in the nozzle plume.

can qualitatively determine the general characteristics of the impact that these instabilities have on cross field transport. In Figure 8, a positive phase velocity implies a diamagnetic drift velocity, while the inverse implies a paramagnetic drift. Here, we observe evidence of both. Diamagnetic drifts seem to exist closer to the thruster, which we expect. However, downstream we observe a change in propagation direction. The paramagnetic drifts will allow inward electron detachment. However, this result may be a result of the presence of the monopole antenna. Its existence in the ionization region provides a physical barrier to plasma transport, implying that the region directly downstream of the antenna will be unlikely to contain a significant plasma presence before diffusivity is enhanced. Thus, the pressure gradient will be radially outward, which will induce a paramagnetic electron drift. As we see in Figure,4, the gradient is indeed radially outwards close to centerline. In an electrodeless MN, this pressure well on centerline does not always exist.

C. Anomalous Collision Frequency

To determine whether the observed instabilities have a significant impact on electron detachment, we must determine the anomalous collision frequency where the wave persists. To do so, we refer to Equation 15. We first determine the frequency components of the ion saturation current, perform a summation up to 250 kHz where we see the waves disappear, then multiply by the plasma frequency throughout the plume.

Figure 11 presents the results from this calculation.

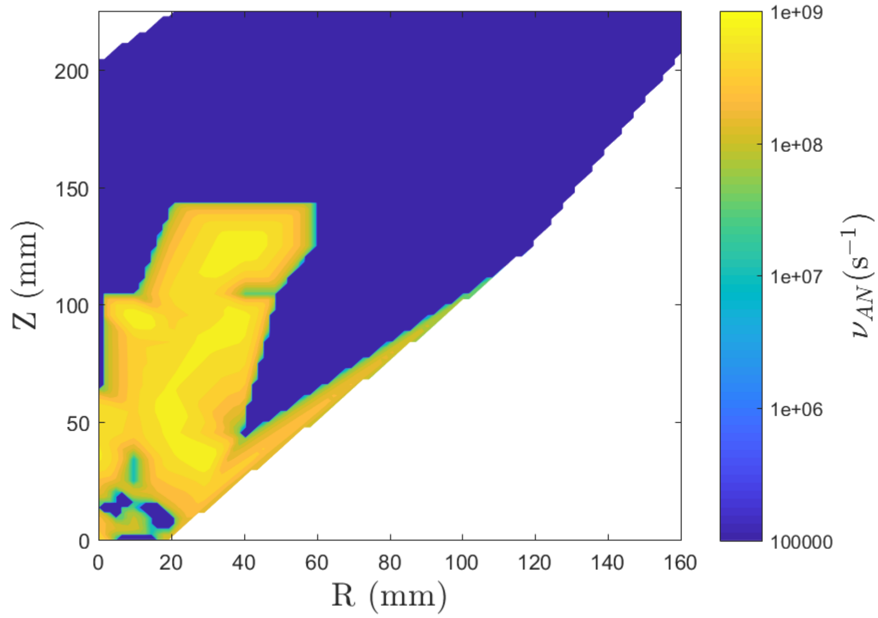

Fig. 11 Anomalous collision frequency estimates (s^{-1}).

We can now compare these values to those produced by classical resistivity by estimating the neutral density throughout the plume. Assuming an electron temperature of 10 eV and an electron-xenon collisional cross section of σ = 20 Å^2 [20], we determine the classical electron-neutral collision frequency as $\nu_c = n_n \sigma \sqrt{T_e/m_e}$. Assuming a low ionization fraction, we assume that the plasma does not affect the neutral density pattern.

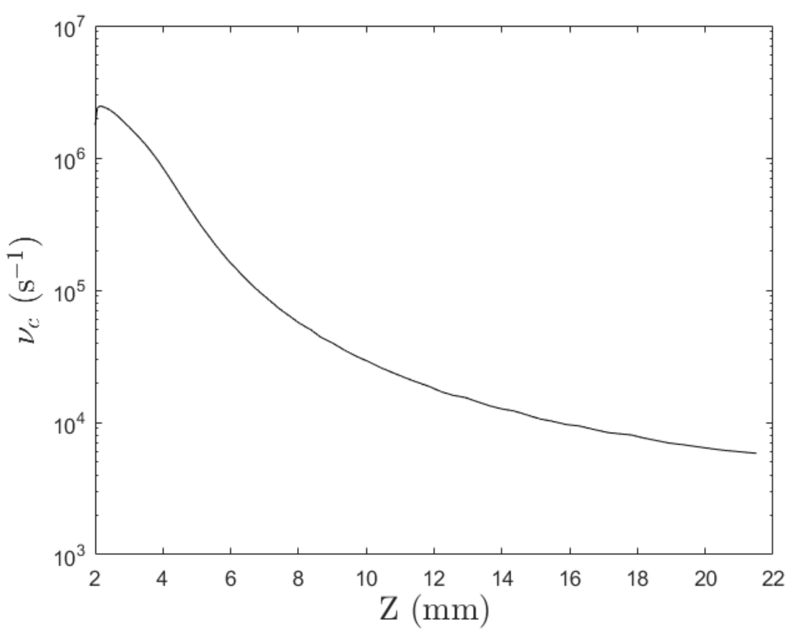

Fig. 12 Estimated classical collision frequencies throughout the plume.

By these estimates, the anomalous collision frequencies remain significant throughout the plume, while the classical collision frequencies will decay downstream from the natural diffusion of the neutral gas. As a higher collision frequency enhances cross field transport, these instabilities may cause electrons to detach.

D. Comparison with Classical Collision Frequency

Resistive detachment by electron-neutral collisions has previously been shown to cause detachment. The anomalous resistivity term can contribute to this effect when the background neutral population is not sufficient. Here, we present the ratio between the anomalous and classical collision frequencies ν_{AN}/ν_C to elucidate the areas where anomalous resistivity becomes the dominant term. Figure 13 presents these ratios.

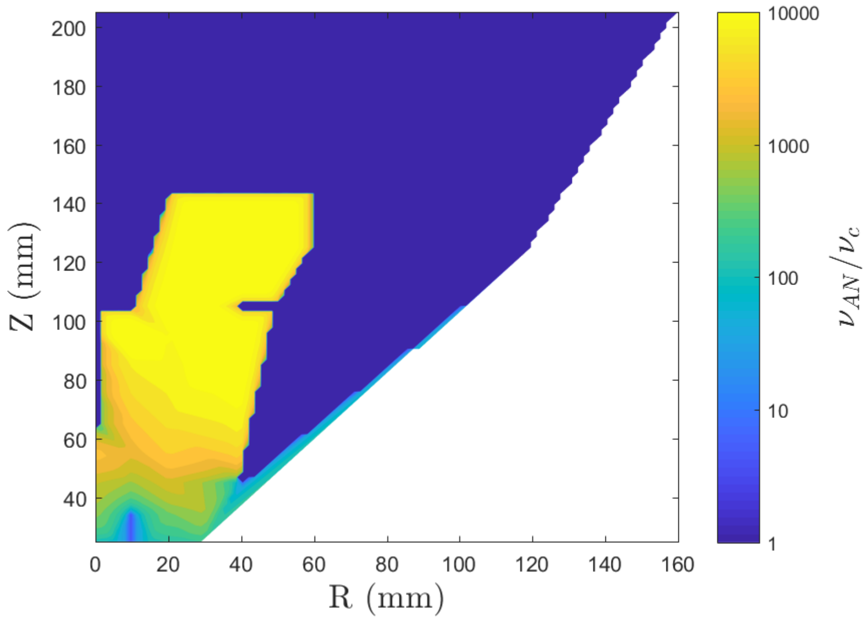

Fig. 13 Ratio of anomalous to electron-neutral collision frequencies throughout the plume.

It is clear from Figure 13 that the anomalous collision frequency induced by these instabilities is generally several orders of magnitude more significant than the electron-neutral collision frequency throughout the plume. Close to the thruster exit plane, the classical collisions remain significant. However, the rise of instabilities downstream quickly becomes the dominant term between the two. While electron-neutral collisions become insignificant downstream, we see a continued wave presence farther downstream.

Our background plasma measurements indicate that detachment has not yet occurred in the region where electron-neutral collisions are significant. We can determine this by noting the presence of a potential and density well on centerline. These wells do eventually disappear throughout the unstable regions, indicating that these instabilities may play a role in inciting downstream detachment.

VII. Conclusion

In this work, we observe a set of plasma instabilities in the plume of a magnetic nozzle using a pair of azimuthally oriented ion saturation probes. To our knowledge, this work represents the first time that such a behavior has been directly observed in such a device. We take these instabilities to be turbulent forms of the electron-cyclotron drift instability and calculate the resulting anomalous collision frequency throughout the plume. Furthermore, we discuss the importance of these instabilities in the context of electron detachment from magnetic nozzles and compare their significance to electron-neutral collisions, finding the former to be much more significant downstream. While we can estimate the effect that these instabilities have by assuming an acoustic-like dispersion, further work is necessary to further specify the enhancement of cross field transport and detachment provided by instability presence.

Acknowledgments

This work was funded under NASA Space Technology and Research Fellowship grant number 80NSSC17K0156.

References

[1] Charles, C., and Boswell, R., "Current-Free Double-Layer Formation in a High-Density Helicon Discharge," *Applied Physics Letters*, Vol. 82, 2003. doi:10.1063/1.1557319, URL `http://dx.doi.org/10.1063/1.1557319http://scitation.aip.org/content/aip/journal/apl/82/9?ver=pdfcov`.

[2] Sheehan, J. P., Collard, T. A., Ebersohn, F. H., and Longmier, B. W., "Initial Operation of the CubeSat Ambipolar Thruster," *30th International Electric Propulsion Conference*, IEPC-2015-243, Hyogo-Kobe, Japan, 2015. URL `http://pepl.engin.umich.edu/pdf/IEPC-2015-243.pdf`.

[3] Winglee, R., Ziemba, T., Giersch, L., Prager, J., Carscadden, J., and Roberson, B. R., "Simulation and Laboratory Validation of Magnetic Nozzle Effects for the High Power Helicon Thruster," *Physics of Plasmas*, Vol. 14, No. 063501, 2007. doi:10.1063/1.2734184, URL `http://dx.doi.org/10.1063/1.2734184http://aip.scitation.org/toc/php/14/6`.

[4] Caruso, N. R. S., "Facility Effects on Helicon Thruster Operation," Ph.D. thesis, Georgia Institute of Technology, 2016. URL `http://hpepl.ae.gatech.edu/papers/CARUSO_DISSERTATION_2016.pdf`.

[5] Merino, M., and Ahedo, E., "Plasma detachment in a propulsive magnetic nozzle via ion demagnetization," *Plasma Sources Science and Technology*, Vol. 23, No. 3, 2014. doi:10.1088/0963-0252/23/3/032001.

[6] Ahedo, E., and Merino, M., "On electron inertia and current ambipolarity in magnetic nozzle models," *International Electric Propulsion Conference*, IEPC-2011-050, Wiesbaden, Germany, 2011. URL `http://erps.spacegrant.org/uploads/images/images/iepc_articledownload_1988-2007/2011index/IEPC-2011-050.pdf`.

[7] Arefiev, A. V., and Breizman, B. N., "Theoretical Components of the VASIMR Plasma Propulsion Concept," *Physics of Plasmas*, Vol. 11, No. 5, 2004. doi:10.1063/1.1666328, URL `http://dx.doi.org/10.1063/1.1666328http://aip.scitation.org/toc/php/11/5`.

[8] Roberson, B. R., Winglee, R., and Prager, J., "Enhanced Diamagnetic Perturbations and Electric Currents Observed Downstream of the High Power Helicon," *Physics of Plasmas*, Vol. 18, No. 053505, 2011. doi:10.1063/1.3574753, URL `http://earthweb.ess.washington.edu/winglee/RecentPapers/2011HighPowerHelicon.pdf`.

[9] Moses, R. W., Gerwin, R. A., and Schoenberg, K. F., "Resistive plasma detachment in nozzle based coaxial thrusters Magnetohydrodynamic scenario of plasma detachment in a magnetic nozzle RESISTIVE PLASMA DETACHMENT IN NOZZLE BASED COAXIAL THRUSTERS," *AIP Conference Proceedings Physics of Plasmas Physics of Plasmas*, Vol. 246, No. 10, 1992, pp. 73501–43504. URL `https://doi.org/10.1063/1.41752http://aip.scitation.org/toc/apc/246/1`.

[10] Collard, T. A., Byrne, M. P., Hepner, S. T., Durot, C. J., and Jorns, B. A., "Investigation of Detachment in a Miniature Magnetic Nozzle Source," *35th International Electric Propulsion Conference*, IEPC-2017-335, Atlanta, Georgia, USA, 2017.

[11] Olsen, C. S., "Experimental Characterization of Plasma Detachment from Magnetic Nozzles," Ph.D. thesis, Rice University, 2013.

[12] Mcdonald, M. S., Bellant, C. K., Pierre, B. A. S., and Gallimore, A. D., "Measurement of Cross-Field Electron Current in a Hall Thruster Due to Rotating Spoke Instabilities," *AIAA/ASME/SAE/ASEE Joint Propulsion Conference & Exhibit*, AIAA 2011-5810, San Diego, CA, 2011. URL `http://pepl.engin.umich.edu/pdf/AIAA-2011-5810.pdf`.

[13] Lafleur, T., Baalrud, S. D., and Chabert, P., "Theory for the anomalous electron transport in Hall effect thrusters. II. Kinetic model Theory for the anomalous electron transport in Hall effect thrusters. I. Insights from particle-in-cell simulations," *Physics of Plasmas Physics of Plasmas Journal of Applied Physics*, Vol. 23, No. 121, 2016. doi:10.1063/1.4972269, URL `https://doi.org/10.1063/1.4948496http://aip.scitation.org/toc/php/23/5`.

[14] Frias, W., Smolyakov, A. I., Kaganovich, I. D., and Raitses, Y., "Long Wavelength Gradient Drift Instability in Hall Plasma Devices. I. Fluid Theory," *Physics of Plasmas II. Applications Physics of Plasmas Journal of Applied Physics*, Vol. 19, No. 8, 2012, pp. 72112–52108. doi:10.1063/1.4736997, URL `http://dx.doi.org/10.1063/1.4736997http://aip.scitation.org/toc/php/19/7`.

[15] Jorns, B. A., and Hofer, R. R., "Plasma Oscillations in a 6-kW Magnetically Shielded Hall Thruster," *Physics of Plasmas*, Vol. 21, No. 5, 2014. doi:10.1063/1.4879819.

[16] Cannat, F., Lafleur, T., Jarrige, J., Chabert, P., Elias, P.-Q., and Packan, D., "Optimization of a coaxial electron cyclotron resonance plasma thruster with an analytical model," *Physics of Plasmas*, Vol. 22, No. 121, 2015. doi:10.1063/1.4972269, URL https://doi.org/10.1063/1.4920966https://doi.org/10.1063/1.4920966.

[17] Beall, J. M., Kim, Y. C., and Powers, E. J., "Estimation of Wavenumber and Frequency Spectra Using Fixed Probe Pairs," *Journal of Applied Physics*, Vol. 53, No. 6, 1982, pp. 3933–3940. doi:10.1063/1.331279.

[18] Wachs, B., and Jorns, B., "Effect of Background Pressure on Ion Dynamics in an Electron Cyclotron Resonance Thruster," *Joint Propulsion Conference*, Cincinnati, 2018.

[19] Sagdeev, R., and Galeev, A., *Nonlinear Plasma Theory*, W.A. Benjamin, 1969.

[20] Subramanian, K. P., and Vijay Kumar, "Total electron scattering cross sections for argon, krypton and xenon at low electron energies," *Journal of Physics B: Atomic and Molecular Physics*, Vol. 20, 1987, pp. 5505–5515. doi:10.1007/BF02847373, URL http://iopscience.iop.org/article/10.1088/0022-3700/20/20/026/pdf.